Available online at www.sciencedirect.com

ScienceDirect

IFAC Papers Online CONFERENCE PAPER ARCHIVE

IFAC PapersOnLine 50-1 (2017) 4478–4483

# Models used for the simulation and control of a segmented ultralight morphing rotor

**Daniel S. Zalkind** * **Lucy Y. Pao** * **Dana P. Martin** ** **Kathryn E. Johnson** **

* *University of Colorado Boulder, Boulder, CO 80309 USA (e-mail: daniel.zalkind@colorado.edu)*

** *Colorado School of Mines, Golden, CO 80401 USA (e-mail: dmartin@mymail.mines.edu )*

**Abstract:** We present the models used in the simulation and control of a segmented, ultralight, morphing rotor (SUMR). These simplified, linear models highlight some differences between the SUMR concept and conventional rotor designs. The models also aid in controller development and turbine design. A baseline controller is presented for the SUMR. To demonstrate how simplified models can be used for system optimization, we present actuator requirements for adequate closed-loop performance. Full, nonlinear, aero-elastic simulations are performed to fine tune the baseline controller for competing objectives. Finally, avenues for future work are outlined.



*Keywords:* Actuators, closed-loop systems, control applications, controlling machines, linear control systems, linearization, proportional plus integral controllers, system models, systems engineering, windmills

## 1. INTRODUCTION

In this paper, we present the models used for simulating and controlling a segmented, ultralight, morphing rotor (SUMR). Our overall goal is to design a 50 MW wind turbine based on the SUMR concept. Economies of scale and offshore development encourage increased rotor sizes, however, blade mass and material costs remain a technological and economical barrier to designing cost-effective, extreme-scale turbines ($> 10$ MW).

The SUMR is inspired by a palm tree; the current concept is a two-bladed, downwind rotor with blades that morph (or cone) downwind so that the aerodynamic, centrifugal, and gravitational forces align along the blade span (Ichter et al., 2016). The current design iteration is an initial 13.2 MW version with a single segment per blade. For each rotor iteration, we will design a baseline controller with the minimum requirements of regulating the rotor speed and maintaining safe load limits according to the international electrotechnical commission (IEC) standards (International Electrotechnical Commission, 2005).

The formulation of accurate models are critical for synthesizing controllers for modern, flexible rotors (Wright, 2004). Simplified models can be used to optimize full wind turbine systems (Hansen and Zahle, 2011; Barlas et al., 2016) and systematically tune gains (Tibaldi et al., 2015), an approach that contrasts with a process that usually requires significant trial-and-error. It is important that the controller is in the loop for these models, so that the effect of disturbances (i.e., wind speed deviations) can be properly analyzed.

We will present linearized models and a baseline controller for the SUMR and compare both with the models and baseline controller for a similar sized conventional design (CONR) and the NREL-5MW reference turbine (Jonkman et al., 2009). Section 2 describes the rotors compared in this study. Section 3 describes the tools used to simulate the SUMR and other turbines. Section 4 presents the linear, state-space models, and the baseline controller is defined in Section 5. In Section 6, we show the results from full, nonlinear system simulations to fine tune the baseline controller. Finally, in Section 7, we outline future uses for these models within the SUMR project.

## 2. TURBINE MODELS

The main properties of the turbines studied in this work are listed in Table 1. Comparing the NREL-5MW to the CONR demonstrates the effect that up-scaling has on the models, e.g., rotor mass increases faster than rated power. The SUMR design differs from the CONR in that it is lighter than the CONR, has a downwind, 2-bladed configuration, and has a variable cone angle.

### *2.1 NREL-5MW Ref. Turbine*

The NREL-5MW reference turbine was developed by the United States National Renewable Energy Laboratory (NREL) and inspired by state-of-the art designs

⋆ This work was supported by the Advanced Research Projects Agency for Energy (ARPA-E) under the Segmented Ultralight Morphing Rotor (SUMR) project (Award Number DE-AR0000667). Any opinions, findings, and conclusions or recommendations expressed in this material are those of the authors and do not necessarily reflect the views of ARPA-E. Support from a Fellowship from the Hanse-Wissenshaftskolleg in Delmenhorst, Germany is also gratefully appreciated.


10.1016/j.ifacol.2017.08.377

Table 1. Turbine Parameters

| Rotor | NREL-5MW | CONR | SUMR |
|---|---|---|---|
| Rated Power | 5 MW | 13.2 MW | 13.2 MW |
| Rated Wind Speed | 11.3 m/s | 11.3 m/s | 11.3 m/s |
| Rated Rotor Speed | 12 rpm | 9.77 rpm | 9.54 rpm |
| Hub Height | 87 m | 142.4 m | 142.4 m |
| Rotor Radius | 62.5 m | 102.5 m | 106.8 m |
| Rotor Position | Upwind | Upwind | Downwind |
| Rotor Mass | 109,660 kg | 392,975 kg | 275,355 kg |
| Number of Blades | 3 | 3 | 2 |
| Blade Mass | 17,740 kg | 49,000 kg | 56,000 kg |
| Mean Chord | 3.48 m | 3.97 m | 4.65 m |
| Cone Angle | -2.5° | -2.5° | 2.5 to 12.5° |

and projects at the time. Their goal was to present a reference for research teams to use for comparing designs, whether they be structurally-, aerodynamically-, or controls-oriented (Jonkman et al., 2009).

### *2.2 Conventional 13.2 MW Ref. Turbine (CONR)*

To make a fair cost of energy analysis, the CONR will be used as a reference for comparing extreme scale wind turbines. The CONR consists of SNL100-03 blades (Griffith and Richards, 2014) in an upwind, 3-bladed configuration.

### *2.3 Segmented Ultralight Morphing Rotor*

The SUMR is a downwind, 2-bladed rotor that does not have a teeter hinge, but instead morphs downwind with cone angle $\beta$ so that the blades more closely align with the load path (Fig. 1). The aerodynamic design of the SUMR is based on an inverse design methodology, where a desired power output is set and the blade chord distribution, twist, and radius are solved to ensure an axial induction factor of 1/3 (Betz limit) along the blade. The airfoils were also

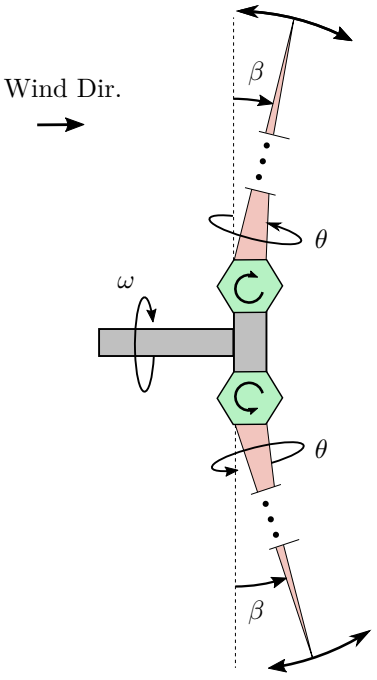


Fig. 1. System model for the SUMR: $\omega$ is the rotor speed, $\theta$ is the collective blade pitch angle, and $\beta$ is the morphing (or coning) angle.

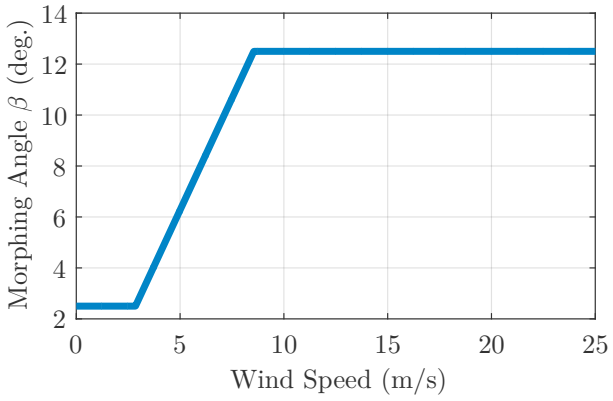


Fig. 2. Morphing schedule for the SUMR

inversely design based on minimum thickness requirements with inputs from the structural design (Ananda, 2016).

The structural design of the SUMR blade is done at Sandia National Laboratories (SNL), using design tools that convert structural layups to distributed parameter and mode shapes for FAST simulations (to be discussed in Section 3). The layup is designed so that maximum load limits do not translate into unacceptable strains or deflections, and to ensure that fatigue resistance is adequate, with the goal to design a blade less than or equal to 56,000 kg (Griffith, 2016).

To enable load alignment, the rotor will be designed to morph depending on mean wind speed. The morphing schedule is shown in Fig. 2; it is a linear ramp from 2.5° at 25% rated wind speed (see Table 1) to 12.5° at 75% of rated wind speed and constant thereafter. Later models may morph up to 30°, and the effects of greater coning angles will be investigated. The morphing degree-of-freedom (DOF) is expected to operate at very slow bandwidths, so during this study it will be assumed to be quasi-steady. The morphing angle will be implemented in each simulation by setting a constant pre-cone angle for all blades according to the mean wind speed.

## 3. SIMULATION AND ANALYSIS TOOLS

A number of computer-aided-engineering tools were used in this study. The latest version of FAST (FAST8) was used to simulate the wind turbine dynamics (Jonkman, 2013). FAST can also do full-system linearizations, which are used to develop reduced-order models in the next section (Jonkman and Jonkman, 2016). Turbsim (Jonkman and Kilcher, 2012) is used to generate the full-field turbulence wind files that are inputs to FAST with a 235 m by 235 m grid and 47 grid elements in each direction.

## 4. SIMPLIFIED TURBINE MODELS

Simplified models will be used in controller design for computing gains, verifying pole positions, and monitoring loop stability. Including the controller (Section 5) in the loop enables us to examine its disturbance rejection properties and the effect that actuators and additional filters have on the system dynamics.

A linear time-varying system of the following form is computed using FAST:

$$\dot{x}(t) = A_P(t)x(t) + B_P(t)u(t) \quad (1)$$
$$y(t) = C_P(t)x(t) + D_P(t)u(t), \quad (2)$$

where $A_P(t), B_P(t), C_P(t)$, and $D_P(t)$ are the state-space matrices of the linearized system at time $t$. Enough time should be simulated to allow the turbine to reach steady state. Linearization times $t$ were selected to evenly space the linearizations over one rotor revolution. When there are no rotating states, e.g., blade states, the matrices, inputs, and outputs can be averaged over $t$, and a linear time-*invariant* system will be used. In these cases, the argument $t$ will be omitted. Each linearization is taken with respect to an operating point. These operating points are determined through steady-state simulations of the rotor using the baseline controller (Section 5).

Because the system is non-linear, the states, inputs, and outputs of the system (1)-(2) represent deviations (denoted using $\delta$) from the operating points. For instance, if the turbine is linearized around the operating points for wind speed $u_{h,op}$, generator torque $\tau_{g,op}$, and collective blade pitch $\theta_{op}$, then the input to the linearized system is

$$u = \left[\delta u_h \;\; \delta\tau_g \;\; \delta\theta\right]^T, \quad (3)$$

where $u_h = u_{h,op} + \delta u_h$ is the *actual* uniform, hub-height wind speed, $\tau_g = \tau_{g,op} + \delta\tau_g$ is the actual generator torque, and $\theta = \theta_{op} + \delta\theta$ is the actual collective blade pitch angle. The input vector $u$ includes both the disturbance ($\delta u_h$) and control inputs ($\delta\tau_g$ and $\delta\theta$). Outputs in (2) are defined similarly and can be any specified FAST output. We will primarily look at the outputs for generator speed $\omega_g$ as well as loads on the blades and tower.

The number of states in (1) and (2) can be changed to model different dynamics of the system. In the following, we will review an input-output description model, a rigid drivetrain model, a flexible drivetrain model, and a flexible blade model.

### *4.1 Input-Output Description*

When there are no states, only the feedthrough matrix $D_P$ remains. If the outputs are

$$y = \left[P \quad T\right]^T, \quad (4)$$

where $P$ and $T$ are the rotor power and thrust, respectively, then

$$D_P = \begin{bmatrix} \partial P/\partial u_h & \partial P/\partial \tau_g & \partial P/\partial \theta \\ \partial T/\partial u_h & \partial T/\partial \tau_g & \partial T/\partial \theta \end{bmatrix}. \quad (5)$$

The entries of this Jacobian are sometimes referred to as the aerodynamic gains and damping of the system.

The term $\partial P/\partial\theta$, the sensitivity of power to pitch, is used to compute the gains of the baseline pitch controller. In Fig. 3, the $\partial P/\partial\theta$ of the NREL-5MW, CONR, and SUMR at different coning angles are compared. As rotor size increases, so does the sensitivity of power to pitch and the sensitivity decreases with increasing cone angles. Since increasing the coning angle decreases power, it is expected that the same change in pitch would have a lesser effect on power when the coning angle is large.

The other terms in (5) can be used in controller and estimator design. For example, $\partial T/\partial\theta$ is used to compute the gain of an active collective-pitch tower-damper (Bossanyi, 2003).

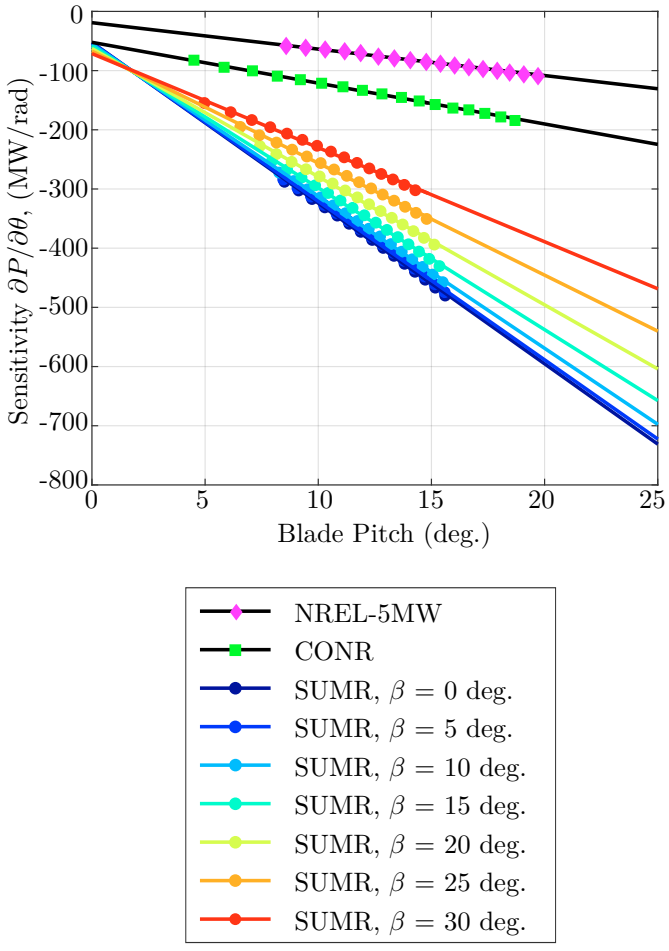


Fig. 3. Comparison of $\partial P/\partial\theta$ in (5) for the NREL-5MW, CONR, and SUMR at various cone angles $\beta$. Each turbine was linearized at pitch angle operating points that correspond to above-rated wind speeds (markers) and fitted with respect to blade pitch (lines).

### *4.2 Rigid Drivetrain*

This model uses the rotor speed deviation

$$x_P = \delta\omega \quad (6)$$

as the only state. This model is used to derive the pitch controller gains in above-rated operation (Section 5). It also allows us to verify the pole locations of the closed-loop system (referred to as the regulator mode) and analytically determine the disturbance rejection of the controller.

### *4.3 Flexible Drivetrain*

In the flexible drivetrain model, the generator and rotor can rotate freely. This introduces $\phi$, the drivetrain torsion angle, i.e., the difference between the generator and rotor angular position. The states are

$$x_P = \left[\delta\omega \;\; \delta\phi \;\; \delta\dot{\phi}\right]^T. \quad (7)$$

The eigenvalues associated with the drivetrain torsion angle are an underdamped conjugate pair. An initial comparison between the NREL-5MW, CONR, and SUMR

showed a highly underdamped torsional mode in the two larger rotors. Linear models with the states in (7) were used to update the lumped spring and damping constants of the physical drivetrain model in FAST to achieve a similar damping ratio and scaled natural frequency as the NREL-5MW model.

### *4.4 Flexible Blades*

Enabling the blade flap-wise DOF in FAST allows the blades to deflect in the flapwise direction. The states in this model are

$$x_P = \left[\delta\omega \;\; \delta\phi \;\; \delta x_{b,1} \dots \delta x_{b,n} \;\; \delta\dot{\phi} \;\; \delta\dot{x}_{b,1} \dots \delta\dot{x}_{b,n}\right]^T, \quad (8)$$

where $x_{b,i}$ is the tip displacement of blade $i$ and there are $n$ blades. The blade modes are *rotating* states; they can be analyzed in the rotating or non-rotating frame. For three-bladed turbines, the multi-blade coordinate (MBC) transformation (Bir, 2008) converts the system to a linear time-*invariant* system, but does not preserve the eigenvalues because the transformation is time periodic. For two-bladed rotors, the dynamics can be fully described by the collective and differential modes (Johnson, 1980)

$$\begin{bmatrix} x_{b,0} \\ x_{b,d} \end{bmatrix} = \frac{1}{2}\begin{bmatrix} 1 & 1 \\ 1 & -1 \end{bmatrix}\begin{bmatrix} x_{b,1} \\ x_{b,2} \end{bmatrix}. \quad (9)$$

The collective blade mode $x_{b,0}$ is non-rotating, but the differential (or teeter) mode $x_{b,d}$ has periodic terms. Since this state transformation is time invariant, the eigenvalues are preserved and do not vary much with blade azimuth. When the collective blade pitch is an input, there are zeros at the poles associated with the teeter mode, implying that this mode is not controllable through collective blade pitch action (Wright, 2004). However, *individual* pitch control has been demonstrated to control these states (van Solingen and van Wingerden, 2015).

The collective blade modes of all three rotor models (Table 2) are similar, despite our hypothesis that the SUMR would have a lower damping ratio. All three rotors were designed using a similar method: to yield stiff enough blades that sufficiently fatigue damage. Centrifugal forces act like a spring, restoring the blade to its equilibrium position while the flapping velocity of the blade alters aerodynamic forces, opposing motion and adding damping to the system (Johnson, 1980). Further analysis will include higher-order blade modes and their *shapes* for control, with the goal of minimizing moment variations along the blade span.

Table 2. Natural frequency and damping ratio of the collective blade modes found using linearization at 15 m/s

| Rotor | Natural Frequency (rad/s) | Damping Ratio (-) |
|---|---|---|
| NREL-5MW | 4.79 | 0.66 |
| CONR | 3.57 | 0.58 |
| SUMR | 4.91 | 0.66 |

### *4.5 Additional Degrees of Freedom*

More DOFs are available to form further models. The tower DOF allows fore-aft and side-to-side motion; these models can be used to design controllers that dampen tower motion, if necessary. The blade edgewise DOF can be included, which is important as in-plane loads increase due to gravity and blade length. Higher fidelity models might include the second-order modes of the blades and tower, but they tend to have lower amplitudes and higher frequencies, limiting their effect on the closed-loop system dynamics. All DOFs will be enabled in FAST8 when doing full, non-linear simulations of the turbine for load analysis.

## 5. CONTROLLER MODELS

A block diagram of the closed-loop system is shown in Fig. 4. The plant can be described by its transfer function

$$P(s) = C_P(sI - A_P)^{-1}B_P + D_P. \quad (10)$$

The poles of the sensitivity function

$$S(s) = \frac{1}{1 + P_{ij}(s)C(s)} \quad (11)$$

are the poles of the closed-loop system, where $i$ is the index of $P(s)$ corresponding to a plant output (controller input) and $j$ is the index of $P(s)$ corresponding to the plant input (controller output). The controller ($C$) will be defined in Section 5.1.

### *5.1 Baseline Control Laws*

The baseline control laws use the same architecture as those in Jonkman et al. (2009) for the NREL-5MW reference turbine controller. The parameters of the baseline control laws are updated for each rotor as a function of the rotor parameters.

*Torque Control* A lookup-table based control law is used to implement torque control in below-rated wind speeds. The goal is to extract as much power from the wind as possible by operating the turbine close to its maximum power coefficient $C_{P,\max}$. The optimal control law is $\tau_g = k\omega_g^2$, where the optimal gain coefficient is

$$k = \frac{\pi\rho R^5 C_P(\beta)}{\lambda_{\text{opt}}^3 G^3}. \quad (12)$$

$\rho$ is the air density, $R$ is the rotor radius, $\lambda_{opt}$ is the optimal tip-speed-ratio, and $G$ is the gearbox ratio. The maximum power coefficient of the SUMR varies with cone angle $\beta$

$$C_P(\beta) = C_{P,0}\cos^2(\beta) \quad (13)$$

where $C_{P,0}$ is the power coefficient when $\beta = 0$.

Transition regions are linear interpolations from cut-in ($\tau_g = 0$) to the optimal control region and from the optimal control region to rated torque (Jonkman et al., 2009). Since the rated torques of the 13.2 MW turbines

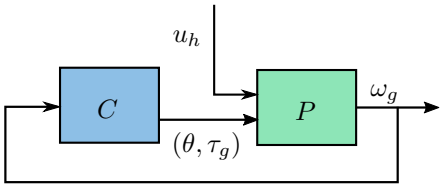


Fig. 4. Block diagram of the simplified turbine-controller system; for the baseline controller $C$, the input to $C$ is generator speed $\omega_g$ and the outputs are generator torque $\tau_g$ and collective blade pitch $\theta$.

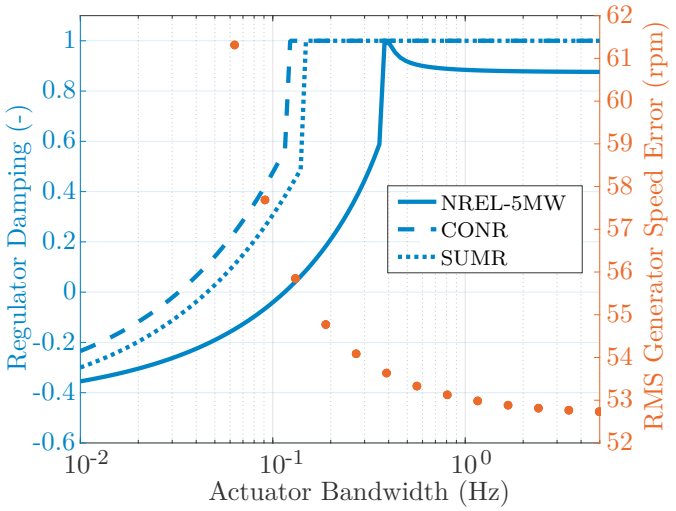


Fig. 5. Regulator mode damping vs. pitch actuator bandwidth $f_{\text{act}}$ for the NREL-5MW, CONR, and SUMR. Also plotted (in red) is the root-mean-squared (RMS) generator speed error from full simulations of the SUMR while varying $f_{\text{act}}$.

are much higher, care must be taken so that the transition is not too steep, effectively yielding a large proportional gain that leads to instabilities.

*Pitch Control* The goal of pitch control is to regulate the generator speed and maintain safe electrical and mechanical load limits. A gain-scheduled, proportional-integral controller is used:

$$\theta_c = k_P(\omega_g - \omega_{g,\text{rated}}) + k_I \int (\omega_g - \omega_{g,\text{rated}})dt, \quad (14)$$

where $\omega_{g,\text{rated}}$ is the rated generator speed, and the $k_P$ and $k_I$ gains are computed based on the desired natural frequency $\omega_n$ and damping ratio $\zeta$ of the generator speed error dynamics (Jonkman et al., 2009):

$$k_P = \frac{2I_{DT}\Omega_0\zeta\omega_n}{G\left[-\frac{\partial P}{\partial \theta}\right]}, \quad (15)$$

$$k_I = \frac{I_{DT}\Omega_0\omega_n^2}{G\left[-\frac{\partial P}{\partial \theta}\right]}. \quad (16)$$

$I_{DT}$ is the drivetrain inertia and $\Omega_0$ is the rated rotor speed. The sensitivity of power to pitch $\partial P/\partial\theta$ is described in (5) and shown in Fig. 3. Since $\partial P/\partial\theta$ varies with blade pitch $\theta$ (and cone angle $\beta$ for the SUMR), the gains in (15) and (16) are scheduled on $\theta$ and $\beta$. This results in closed-loop poles (for the regulator mode) that have a natural frequency near $\omega_n$ and damping ratio near $\zeta$ for all wind speeds above rated. Increasing the natural frequency results in better regulation of the generator speed error. However, reducing the natural frequency reduces the blade loads. These competing objectives require a compromise.

### 5.2 Actuator Dynamics and Filters

A pitch actuator model should be included in the closed-loop dynamics to more accurately represent the system. To model the pitch actuator, we use a second-order, critically damped low-pass filter with a bandwidth $f_{\text{act}}$.

Actuator requirements will be considered in a cost analysis: a faster actuator is expected to cost more, but a slower actuator provides poor generator regulation. The linear models previously described can be used to quickly determine what actuator speed is necessary for adequate control. We show the damping ratio of the regulator mode for different actuator speeds in Fig. 5. For reference, full non-linear simulations of the SUMR were performed and good agreement between regulator damping and generator regulation is seen. A low damping ratio corresponds to poor generator regulation and even controller instability. Beyond a certain actuator bandwidth $f_{\text{act}}$, diminishing returns in performance are observed. A good choice of $f_{\text{act}}$ would be right before this point of diminishing returns. The smaller NREL-5MW turbine requires a faster actuator because the generator response to a disturbance is faster, though the chosen regulator frequency $\omega_n$ has a strong relation to the necessary actuator bandwidth $f_{\text{act}}$.

Filters are used to remove high-frequency content from control signals. In our baseline controller, only a single-order low-pass filter with a bandwidth of 0.5 Hz was used. These filters are added into the control law $C(s)$ to determine the system performance in terms of the linear models.

## 6. NONLINEAR AEROELASTIC SIMULATIONS

Ultimately, full, non-linear simulations are used to verify turbine performance. When *all* of the DOFs are enabled, this provides the most realistic estimate of turbine loads for certification purposes. We use these simulations to tune the pitch controller. A full system analysis would include all component load limits, but our current goal is to reduce blade mass by reducing the reinforcements necessary for mitigating blade *flap-wise* fatigue and extreme loads. The regulator mode parameters $(\omega_n, \zeta)$ were varied to reduce the blade flap-wise root bending moment, with the constraint that the generator speed could not exceed 110% of the rated value.

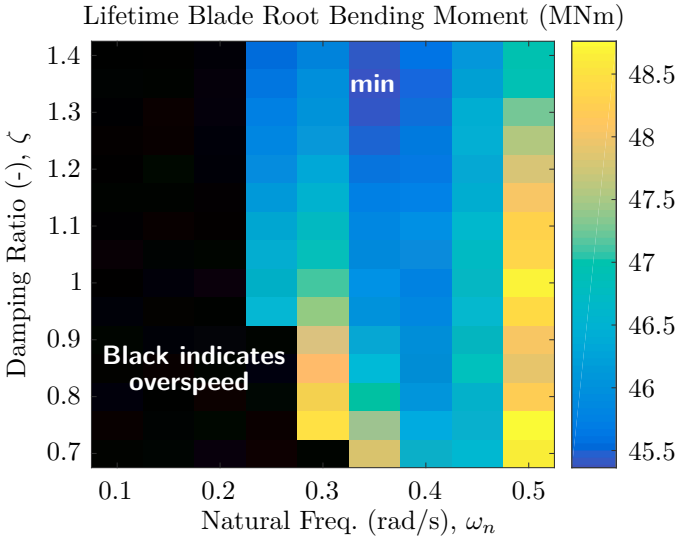


Fig. 6. Lifetime-weighted blade root bending moments for various $\omega_n$ and $\zeta$ choices for the desired regulator mode constrained by maximum generator speeds that do not exceed 110% of the rated value.

Simulations were carried out on a subset of the design load case (DLC) 1.2 (normal turbulence, fatigue loads), using three wind fields with mean wind speeds of 12, 16, and 20 m/s (International Electrotechnical Commission, 2005). The results are shown in Fig. 6, which suggests gains (using $\omega_n = 0.35$ rad/s, $\zeta = 1.35$) that minimize blade loads while satisfying generator overspeed constraints. A more holistic approach to controller tuning would weigh the *economic* cost of loads on more components and include design envelopes as constraints.

## 7. DISCUSSION AND NEXT STEPS

It is important to note that this is a starting point for controls research on the SUMR. Several extensions and improvements should be included in future research.

As a benchmark for comparison, the CONR was simulated for several DLCs. The results, summarized in Fig. 7, highlight some of the challenges for large rotors. During normal operation, in-plane blade loads are higher due to gravitational loads. Normally out-of-plane blade loads are the target for blade load reduction in controls research. This suggests that the controller used in normal operation should focus on whether these *in-plane* blade loads are controllable and, if so, how? However, during extreme events, the out-of-plane blade loads are higher. Since ultimate strength will also be explored as part of this project, another objective should be the reduction of out-of-plane blade loads. Load reductions enable lighter (and less expensive) blade designs. More advanced control methods will be attempted using the previously described models (Section 4), including individual pitch control, and active drivetrain and tower dampers. Ultimately, morphing dynamics will also be included, as well as the structural dynamics associated with segmented blades.

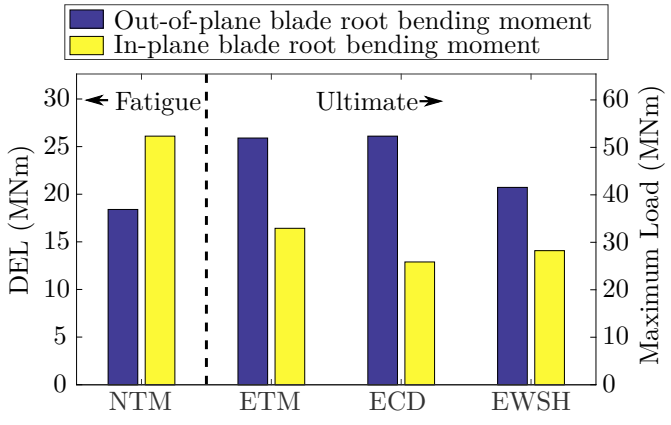


Fig. 7. Summary of DLC results for the CONR following the IEC standard method for load calculations (International Electrotechnical Commission, 2005). This includes the damage equivalent loads (DELs) for the fatigue analysis during normal operation and turbulence (NTM, left) and the maximum loads (right) during extreme turbulence (ETM), extreme change in wind direction (ECD) and extreme wind shear (EWSH) for the in-plane (yellow) and out-of-plane (blue) blade root bending moments.

These will pose interesting challenges from a controls perspective.

## ACKNOWLEDGEMENTS

We would like to acknowledge all who helped in the design of the initial SUMR. Gavin Ananda, Suraj Bansal, and Michael Selig provided the aerodynamic definition for the rotor. D. Todd Griffith provided the structural blade properties. Carlos Noyes and Eric Loth provided the initial morphing schedule.

## REFERENCES

Ananda, G. (2016). Personal communication.
Barlas, A.K., Tibaldi, C., Zahle, F., and Madsen, H.A. (2016). Aeroelastic Optimization of a 10 MW Wind Turbine Blade with Active Trailing Edge Flaps. In *AIAA*.
Bir, G. (2008). Multiblade Coordinate Transformation and Its Application to Wind Turbine Analysis. In *AIAA*.
Bossanyi, E. (2003). Wind turbine control for load reduction. *Wind Energy*, 6, 229–244.
Griffith, D.T. (2016). Personal communication.
Griffith, D.T. and Richards, P.W. (2014). The SNL100-03 Blade : Design Studies with Flatback Airfoils for the Sandia 100-meter Blade. Tech. Rep. SAND2014-18129, SNL.
Hansen, M. and Zahle, F. (2011). Aeroelastic Optimization of MW Wind Turbines. Tech. Rep. Risø-R-1803, Risø DTU National Laboratory for Sustainable Energy.
Ichter, B., Steele, A., Loth, E., Moriarty, P., and Selig, M. (2016). A morphing downwind-aligned rotor concept based on a 13-MW wind turbine. *Wind Energy*, 19(4), 625–637.
International Electrotechnical Commission (2005). IEC 61400-1: Wind Turbines.
Johnson, W. (1980). *Helicopter Theory*. Princeton University Press, Princeton, N.J.
Jonkman, B. and Kilcher, L. (2012). TurbSim User's Guide: Version 1.06.00. Tech. Rep., NREL.
Jonkman, J.M. and Jonkman, B.J. (2016). FAST modularization framework for wind turbine simulation: full-system linearization. In *The Science of Making Torque from Wind*.
Jonkman, J. (2013). The New Modularization Framework for the FAST Wind Turbine CAE Tool. In *AIAA*.
Jonkman, J., Butterfield, S., Musial, W., and Scott, G. (2009). Definition of a 5-MW Reference Wind Turbine for Offshore System development. Tech. Rep. NREL/TP-500-38060.
Tibaldi, C., Hansen, M.H., and Zahle, F. (2015). Methods for systematic tuning of wind turbine controllers. Tech. Rep. DTU Wind Energy E-0100.
van Solingen, E. and van Wingerden, J.W. (2015). Linear individual pitch control design for two-bladed wind turbines. *Wind Energy*, 18, 677–697.
Wright, A.D. (2004). Modern Control Design for Flexible Wind Turbines. Tech. Rep. NREL/TP-500-35816.